



Planetary Engulfment in the Hertzsprung–Russell Diagram

Morgan MacLeod^{1,4} , Matteo Cantiello^{2,3} , and Melinda Soares-Furtado³

¹ Harvard-Smithsonian Center for Astrophysics, 60 Garden Street, Cambridge, MA 02138, USA; morgan.macleod@cfa.harvard.edu

² Center for Computational Astrophysics, Flatiron Institute, 162 5th Avenue, New York, NY 10010, USA

³ Department of Astrophysical Sciences, Princeton University, Princeton, NJ 08544, USA

Received 2017 December 4; revised 2018 January 5; accepted 2018 January 7; published 2018 January 16

Abstract

Planets accompany most Sun-like stars. The orbits of many are sufficiently close that they will be engulfed when their host stars ascend the giant branch. This Letter compares the power generated by orbital decay of an engulfed planet to the intrinsic stellar luminosity. Orbital decay power is generated by drag on the engulfed companion by the surrounding envelope. As stars ascend the giant branch their envelope density drops and so does the power injected through orbital decay, scaling approximately as $L_{\text{decay}} \propto R_*^{-9/2}$. Their luminosity, however, increases along the giant branch. These opposed scalings indicate a crossing, where $L_{\text{decay}} = L_*$. We consider the engulfment of planets along isochrones in the Hertzsprung–Russell (H–R) diagram. We find that the conditions for such a crossing occur around $L_* \approx 10^2 L_\odot$ (or $a \approx 0.1$ au) for Jovian planetary companions. The consumption of closer-in giant planets, such as hot Jupiters, leads to $L_{\text{decay}} \gg L_*$, while more distant planets such as warm Jupiters, $a \approx 0.5$ au, lead to minor perturbations of their host stars with $L_{\text{decay}} \ll L_*$. Our results map out the parameter space along the giant branch in the H–R Diagram where interaction with planetary companions leads to significant energetic disturbance of host stars.

Key words: planet–star interactions – planetary systems – stars: evolution

1. Introduction

Planetary companions to extrasolar stars have been uncovered in great abundance by transit and radial velocity searches (Winn & Fabrycky 2015). The discovery of numerous giant planets in compact orbits beginning with 51 Peg b (Mayor & Queloz 1995) was unexpected given the architecture of our own solar system (Howard et al. 2012; Wright et al. 2012). About 10% of approximately solar-mass stars host giant planets with orbital periods of a few years or less (Winn & Fabrycky 2015). Of these, some are in very compact orbits of days (hot Jupiters, $a \lesssim 0.1$ au), while others populate longer orbital periods (warm Jupiters, $0.1 \text{ au} \lesssim a \lesssim 1$ au). More massive substellar companions like brown dwarfs are found to be nearly an order of magnitude less common than giant planets at these orbital separations (Grether & Lineweaver 2006).

As stars evolve, their radii grow significantly. Planetary companions with orbital separations less than au scales can be engulfed within the envelopes of their growing giant-star hosts (e.g., Villaver & Livio 2009; Schlaufman & Winn 2013). During the ensuing common envelope phase, the orbit of the companion shrinks in response to drag generated by interaction with the surrounding envelope (Paczynski 1976). The deposition of orbital energy is a power source within the stellar envelope. Depending on the relative magnitude of this power source and the nuclear-burning power already transported by radiation and convection through the stellar envelope, this addition may represent a perturbation or a large-scale disturbance.

A number of authors have considered the impact of digested planets on their host stars. Several have studied the gas dynamics of planet engulfment (Sandquist et al. 1998; Staff et al. 2016) or the subsequent stellar evolution (e.g., Soker et al. 1984; Siess & Livio 1999a, 1999b; Metzger et al. 2017). Others have discussed the role of digested planets in depositing

angular momentum into the stellar envelope and enhancing stellar rotation (Soker 1998; Siess & Livio 1999b; Zhang & Penev 2014; Privitera et al. 2016a, 2016b), enhancing surface magnetic field (Privitera et al. 2016c), and polluting surface abundances with planetary material (Sandquist et al. 1998; Siess & Livio 1999b; Sandquist et al. 2002; Aguilera-Gómez et al. 2016a, 2016b). Finally, some authors have estimated the role of engulfment events in producing transients from stellar ejecta (Soker & Tytenda 2006; Metzger et al. 2012; Yamazaki et al. 2017), or in shaping planetary nebulae from ejecta (De Marco & Soker 2011).

This work examines one aspect of the broader question of planetary engulfment: the comparison of orbital decay power to stellar luminosity. In Section 2, we outline the scalings that determine the rate at which an engulfed object’s orbit decays in response to interaction with a giant star’s gaseous envelope. In Section 3, we apply these scalings across stellar isochrones to consider interactions characterized by different star and companion populations in the Hertzsprung–Russell (H–R) diagram. We show that the orbital decay power drops with more extended host stars, while the intrinsic stellar power grows, and highlight the presence of a crossing in the relative importance of these two terms. In Section 4, we discuss some implications of our findings in light of previous work, and in Section 5, we summarize our findings.

2. Orbital Decay Power

We begin by considering a system composed of a giant star of mass M_* , with core mass M_c , total radius R_* , and luminosity L_* , and a lower-mass companion of mass M_2 and radius R_2 on a circular orbit. Interaction between the star and planet begins when the star fills its Roche lobe and continues while the orbital separation shrinks until the planet is eroded. During the initial engulfment, the orbital separation is, therefore, similar to

⁴ NASA Einstein Fellow.

the stellar radius. When $a = R_*$, the orbital energy is

$$E_{\text{orb}} = \frac{GM_*M_2}{2R_*}, \quad (1)$$

the orbital velocity is

$$v_{\text{orb}} = \left[\frac{G(M_* + M_2)}{R_*} \right]^{1/2}, \quad (2)$$

and the associated orbital period is

$$P_{\text{orb}} = 2\pi \left[\frac{R_*^3}{G(M_* + M_2)} \right]^{1/2}. \quad (3)$$

The orbit decays in response to a drag force F_d , directed in opposition to the relative motion between the object and the gas, v_{rel} . This force transfers energy from the orbit to the stellar gas at a rate of

$$\begin{aligned} L_{\text{decay}} &= F_d v_{\text{rel}}, \\ &\approx F_d v_{\text{orb}}, \end{aligned} \quad (4)$$

where the second approximation is valid when the surrounding gas is not synchronized with the orbital motion ($v_{\text{rel}} \approx v_{\text{orb}}$, which we adopt below). The drag force can be expressed in the form

$$F_d = C_d A \rho v_{\text{rel}}^2, \quad (5)$$

where A is a cross-sectional area, ρ is the density of the intervening material, and C_d is a dimensionless drag coefficient.

The drag force experienced by an engulfed object depends on whether the appropriate cross section, A , is geometrically or gravitationally determined. The minimum cross section is geometric, πR_2^2 . This cross section is enhanced by gravitational focusing when the escape velocity of the object, $\sqrt{2GM_2/R_2}$, is larger than the relative velocity.⁵ For companions of approximately Jupiter mass and below interacting with stars, the geometric cross section is appropriate and we adopt it here.

We approximate the density in Equation (5) as proportional to the average density of the entire star:

$$\rho \approx \eta \bar{\rho}(R_*) = \eta \frac{3M_*}{4\pi R_*^3}. \quad (6)$$

Within the envelope of an evolved star, $\rho < \bar{\rho}$ (or $\eta < 1$) because mass is concentrated in the stellar core. Figure 1 shows a profile $\rho(r)/\bar{\rho}(r)$ within the interior of a $1.1 M_\odot$ star as it evolves up the giant branch ($r < R_*$). Within the envelope a typical $\eta = \rho(r)/\bar{\rho}(r) \approx 0.1$.

Combining these ingredients yields

$$L_{\text{decay}} \approx \frac{3}{4} C_d \eta G^{3/2} R_2^2 M_* (M_* + M_2)^{3/2} R_*^{-9/2}. \quad (7)$$

We adopt $C_d = 1$ and $\eta = 0.1$ in what follows. The number of orbits over which this orbital decay occurs is

$$N_{\text{decay}} \approx \frac{E_{\text{orb}}}{L_{\text{decay}} P_{\text{orb}}}, \quad (8)$$

which scales as $N_{\text{decay}} \propto (M_2/M_*)(R_*/R_2)^2$ for $M_* \gg M_2$.

⁵ In the limit where it dominates, the gravitational focus cross section, πR_a^2 , depends on the object's mass (rather than its radius) through the gravitational focusing impact parameter $R_a = 2GM_2/v_{\text{rel}}^2$ (Hoyle & Lyttleton 1939).

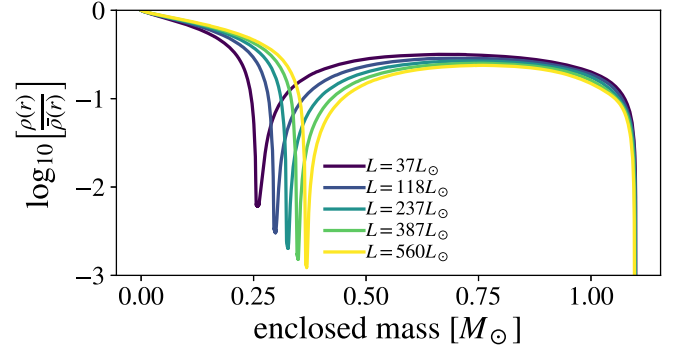


Figure 1. Ratio of density $\rho(r)$ to enclosed average density, $\bar{\rho}(r) = m(r)/(4/3\pi r^3)$, within the envelope of a $1.1 M_\odot$ star as it evolves up the giant branch approximately 8 Gyr after zero-age main sequence. Lines are labeled by stellar luminosity, but growing core mass can also be observed by the dip in $\rho/\bar{\rho}$. The stellar profiles are computed with MESA version 7503 (Paxton et al. 2011, 2013, 2015), with parameters from MESA Isochrones and Stellar Tracks (Choi et al. 2016). We find that $\rho(r)/\bar{\rho}(r) \approx 0.1$ across much of the giant's envelope, without substantial variation as the star evolves.

The above estimates consider the initial plunge and inspiral of the planetary companion within the stellar envelope. This is reasonable, because in generating an order unity change in the orbital energy, the planet intersects a column of mass similar to its own mass, with the likely result being the erosion and disintegration of the planet (Sandquist et al. 1998, 2002). If a planet could inspiral to greater depth before being eroded, the larger mean density and higher orbital velocity imply that L_{decay} would exceed our estimate that considers $a \approx R_*$.

3. Engulfment in the H–R Diagram

In this section we examine how the orbital decay power estimated in the previous section compares to the intrinsic luminosity of evolving giant stars. Because L_{decay} decreases as stars evolve up the giant branch while L_* increases, we find that the relative energetics of consuming a planetary companion depend highly on the star's evolutionary state, and therefore its location in the H–R diagram.

To facilitate this comparison, we use stellar data tabulated by the MESA⁶ Isochrones and Stellar Tracks (MIST) project⁷ (Choi et al. 2016). We use isochrones of solar metallicity, non-rotating post-main-sequence stars, which are available for download among MIST's model grids.

We begin by examining the ratio of orbital decay power generated by the engulfment of a Jovian giant planet ($R_2 = 6.99 \times 10^9$ cm) to intrinsic stellar luminosity. Figure 2 shows this ratio along post-main-sequence isochrones of 10^8 , 10^9 , and 10^{10} year age in the H–R diagram. The ratio of orbital decay power to stellar luminosity spans nearly 10 orders of magnitude across the H–R diagram. We find that near the main-sequence turnoff, where orbits are compact, the associated orbital decay timescale is short, and the power injected through digestion of a giant planet is large compared to the nuclear-burning luminosity of the star. At the tip of the giant branch, the opposite is true and the initial orbital decay of a giant planet within the envelope would result in a small perturbation to the intrinsic stellar luminosity.

Conditions where orbital decay power and stellar luminosity are similar mark a critical transition between stars that could be

⁶ <http://mesa.sourceforge.net/>

⁷ <http://waps.cfa.harvard.edu/MIST/>

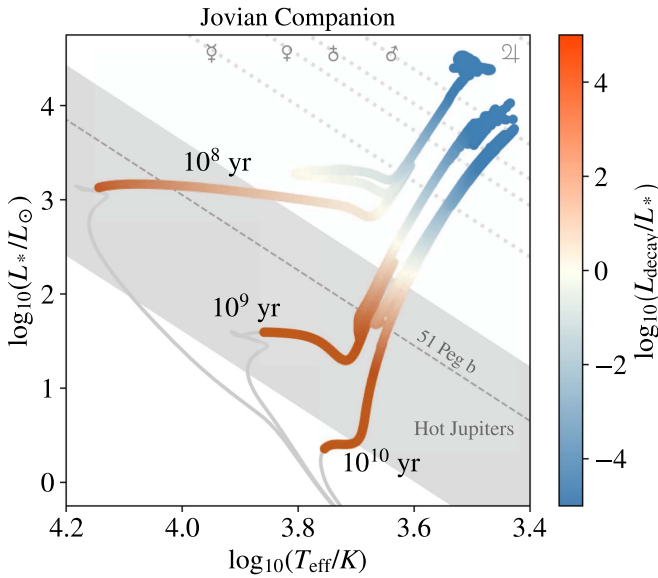


Figure 2. Initial orbital decay power, Equation (7), compared to the intrinsic stellar luminosity. We plot the ratio of L_{decay}/L for solar metallicity, non-rotating stars with isochrone ages 10^8 , 10^9 , and 10^{10} years. In the background the orbital parameters of the inner solar system planets and of hot Jupiters are plotted. A Jovian planet engulfed by a star at the tip of the giant branch (or, equivalently, one at several au separation) has minimal impact on the power output of its host star. In the opposite case, a close-in Jovian planet, such as a hot Jupiter, will deposit orders of magnitude more power in orbital decay than the intrinsic luminosity of a compact host star near the giant-branch turnoff.

largely undisturbed by swallowing a giant-planet companion to those whose structure would be dramatically modified. For stars of 10^{10} year age, the transition occurs about halfway up the giant branch around luminosities of $100 L_{\odot}$.

Locations in the L_* , T_{eff} axes of the H–R diagram map to a radius through an assumption of blackbody emission, $R_*^2 = L_*/4\pi\sigma T_{\text{eff}}^4$. These radii can be compared to the orbital separations of populations of planets. Figure 2 reveals that when a star engulfs a hot Jupiter companion (with, for example, $a \approx 0.05$ au), we expect a dramatic imprint on the host star, with L_{decay} hundreds of times L_* . On the other hand, the engulfment of a typical warm Jupiter (with 0.5 au separation) will result in a minor disturbance to a typical host star with L_{decay} only at the percent level of L_* .

In Figure 3, we extend this consideration of the critical condition. We compute the minimum radius companion that yields $L_{\text{decay}} = L$. The minimum radius is only about 10 km near the main-sequence turnoff, but quickly grows to the size of low-mass rocky planets at hundredths of an au. By $a \approx 0.1$ au, the critical radius is similar to the radius of Jupiter, as can be inferred from Figure 2. Going to the tip of the giant branch the critical radius becomes so large (greater than R_{\odot}) that the object in question would be stellar mass rather than planetary mass. Under those circumstances, gravitational focusing dominates the cross section as discussed in Section 2, and it is the mass, rather than the radius, of the companion that is constrained.

Finally, we examine the number of orbital periods over which an engulfed planet’s orbit decays. The left panel of Figure 4 plots N_{decay} for engulfed Jovian planets; the right panel considers the minimum radius object ($L_{\text{decay}} = L_*$) of Figure 3. Jovian planets undergo orbital decay (and, as noted earlier, likely ablation on a similar timescale) over about 1 orbit near the giant-branch turnoff to about 10^4 orbits near the giant-branch tip. This highlights, in part, why L_{decay}/L_* is so varied

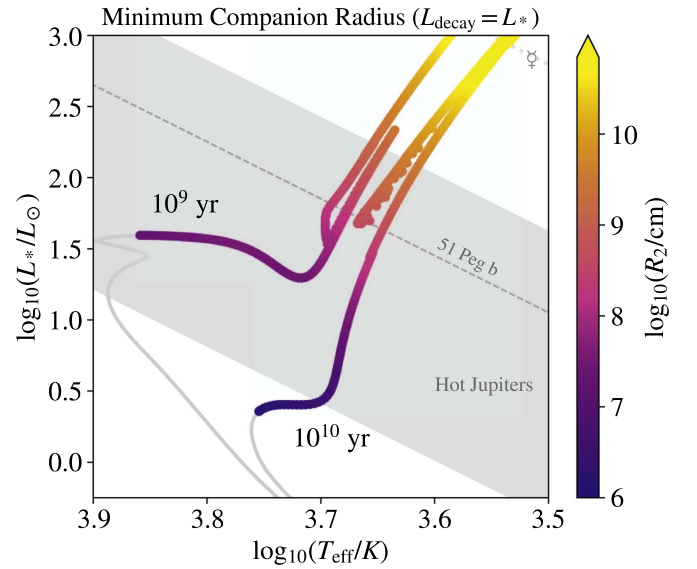


Figure 3. Minimum radius of a companion whose initial orbital decay power matches the intrinsic stellar luminosity, $L_{\text{decay}} = L_*$. Here, we focus on the lower giant branch of 10^9 and 10^{10} year isochrones. Near the main-sequence turnoff, objects as small as 10 km radius can have $L_{\text{decay}} \approx L_*$. The critical radius quickly grows to roughly an Earth radius at hundredths of an au and Jupiter radius at 0.1 au.

across the H–R diagram, the number of orbits over which the orbital energy is dissipated varies significantly. Minimum radius objects can have extraordinarily small $N_{\text{decay}} \approx 10^{-4}$ near the giant-branch turnoff. This indicates that the net injected energy (approximately E_{orb}) is small, and that, in some cases, these objects are so vulnerable that they likely would not survive interaction with a host star’s extended atmosphere to become truly engulfed.

4. Discussion

Having established the comparison of L_{decay} to L_* we discuss its interpretation below.

4.1. Emergent Luminosity versus Orbital Decay Power

Because orbital decay power is generally deposited into very optically thick stellar envelope material, the emergent luminosity is mediated by transport to the stellar photosphere. Nonetheless, orbital decay power can give rise to both short- and long-term electromagnetic emission.

Upon engulfment of a companion, immediate signatures may include cooling emission from shock-heated ejecta (Metzger et al. 2012; Yamazaki et al. 2017) and radio afterglows from ejecta–interstellar medium interactions (Yamazaki et al. 2017). On a dynamical timescale the stellar envelope expands to return to quasi-hydrostatic equilibrium as orbital decay does work against the gravitational binding energy of the envelope. Staff et al. (2016) model the interaction of RGB and AGB stars near the middle and tip of the giant branch with a 10 Jupiter-mass planet and find mild hydrostatic expansion of the objects post-engulfment (along with some, marginally resolved, ejecta). Because these simulations do not model photospheric cooling, this expansion reflects the return to a perturbed hydrostatic equilibrium following the deposition of orbital decay energy.

Longer-term signatures include the eventual transport of heat deposited within layers of the envelope to the stellar surface. The emergent luminosity in this phase is $\Delta L \approx \Delta E(r)/t_{\text{KH}}(r)$,

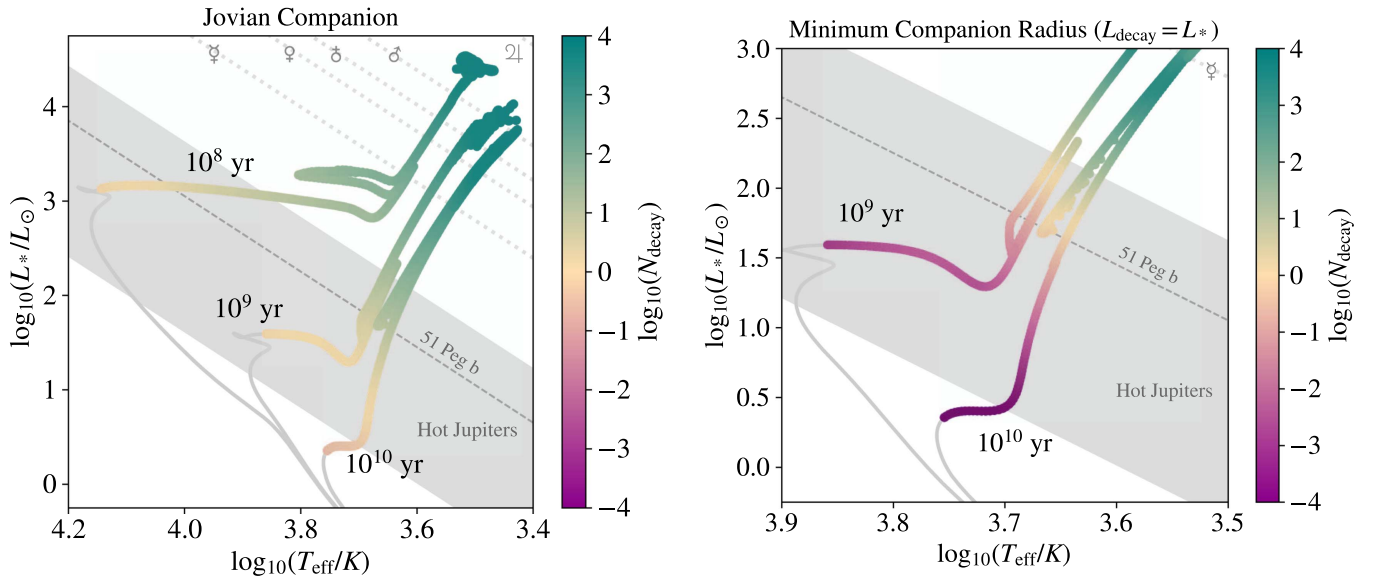


Figure 4. Number of orbits over which engulfed planet’s orbits decay. The left panel considers a Jovian planet, while the right panel considers an object with the minimum radius of Figure 3 and Jovian density. Higher up the giant branch, it takes many orbits for an object’s orbit to decay. Near the turnoff, it takes of order one orbit for an engulfed Jovian planet’s orbit to decay and a minimum size engulfed body’s orbit decays in a tiny fraction of an orbital period. This indicates that these small engulfed objects survive only briefly within their host star’s atmosphere.

where $\Delta E(r)$ is the locally deposited energy and $t_{\text{KH}}(r)$ is the local Kelvin–Helmholtz, or transport, timescale (by convection or radiative diffusion) for that energy through the perturbed stellar envelope structure.

When the orbital decay timescale is short compared to that of energy transport, the initial response of the stellar envelope is expansion, and luminosity emerges only on the longer timescale of energy transport. This implies that cases where $L_{\text{decay}} \gg L_*$ will have net emergent luminosity lower than L_{decay} but higher than L_* . When the timescale for energy transport is short compared to deposition, radiative cooling from the photosphere moderates the extra energy from orbital decay. For example, if cooling were included in the AGB model of Staff et al. (2016), radiation from the photosphere would carry away energy at a similar rate to deposition.

Finally, we note that under the simplifying assumption that orbital decay energy is distributed spherically, the quasi-hydrostatic aspect of energy transport can be addressed in 1D simulations with stellar evolution codes (see, for example, recent calculations presented by Metzger et al. 2017).

4.2. Engulfment and Stellar Rotation

In addition to energy, orbital decay also deposits angular momentum into stellar envelope material. Prior to engulfment, a planet’s orbit may decay through tidal interaction with the host star (e.g., Zahn 1977; Hut 1980; Rasio et al. 1996), in which case much of the angular momentum is expected to be deposited into the host star’s convective zone (Valsecchi & Rasio 2014; Meynet et al. 2017). Stellar evolution calculations including tidal interactions and the uncertain physics of internal angular momentum transport (Privitera et al. 2016b) support the notion that planet engulfment could be responsible for some of the observed fast rotating red giants (Carlberg et al. 2009, 2012). The distribution of angular momentum deposition following engulfment is considerably less certain (though see the characterization of Staff et al. 2016 for their simulated cases).

A related signature of planetary engulfment that is often considered together with enhanced rotation is anomalous surface abundances, in particular Lithium enrichment (e.g., Alexander 1967; Siess & Livio 1999b). However, due to the fragile nature of Lithium, this particular signature is likely short-lived and degenerate with other mixing processes (Privitera et al. 2016b).

4.3. Companion Engulfment Rates

To estimate the rate at which planets are engulfed as their host stars ascend the giant branch, we consider the occurrence rate of close-in planets and the rate at which stars evolve off of the main sequence. The current rate at which $1M_{\odot}$ stars become giants reflects the Milky Way star formation history of approximately 10^{10} years, a main-sequence lifetime, ago. The star formation rate of Milky Way progenitor stars 10^{10} years ago, at approximately redshift 2, has been inferred to be approximately $10 M_{\odot} \text{ yr}^{-1}$ (van Dokkum et al. 2013). Planet occurrence rates vary by planetary and stellar type. Among the *Kepler* sample, approximately 10% of stars host giant planets, while roughly 1% host close-in hot Jupiters (e.g., Winn & Fabrycky 2015). The rate of engulfment in the Milky Way can then be written

$$R_{\text{engulf}} \approx f_{\text{comp}} R_{\text{evol}}, \quad (9)$$

where f_{comp} is the companion occurrence fraction, and R_{evol} is the rate at which stars evolve off the main sequence. For the typical parameters listed above, we therefore find $R_{\text{engulf}} \approx 0.1\text{--}1 \text{ yr}^{-1}$ in the Galaxy depending on what type of companion is considered (see Metzger et al. 2012 for a more detailed discussion including the possibility of planet migration). We note that this rate is similar to the inferred Galactic rate of stellar mergers (Kochanek et al. 2014).

5. Summary

Planets may be engulfed by their evolving host stars when these stars expand on the giant branch. We have compared the power from planetary orbital decay to stellar luminosity across the H–R diagram. Some key considerations are as follows.

1. Drag forces cause the orbit of an engulfed planet to decay, as estimated in Equations (5) and (7), respectively.
2. Whether or not the engulfment of a planet will significantly perturb a giant-branch star’s energetics depends on the properties of the planet (mass, separation) and on the stellar luminosity when it evolves to $R_* \approx a$. The orbital decay power falls steeply with increasing stellar size because the stellar envelope density goes down (roughly $L_{\text{decay}} \propto R_*^{-9/2}$), while luminosity grows sharply with radius in low-mass giants, roughly $L_* \propto R^{3/2}$ (Joss et al. 1987). These opposed scalings indicate the presence of a crossing, where in some conditions $L_{\text{decay}} > L_*$ and in others $L_{\text{decay}} < L_*$.
3. Giant planets on orbits with $a \lesssim 0.1$ au give rise to $L_{\text{decay}} \gg L_*$. Those on wider orbits have $L_{\text{decay}} \ll L_*$ (Figure 2). This indicates that hot Jupiters substantially affect their host stars upon engulfment, while warm Jupiters ($a \approx 0.1$ –1 au) do not. Evolved stars of 10^9 to 10^{10} year age and $L \approx 10^2 L_\odot$ represent the transition population where $L_{\text{decay}} \approx L_*$ for a Jovian planet.
4. We compute the radius of objects that match the critical condition $L_{\text{decay}} = L_*$. These are as small as $R_2 \approx 10$ km for host stars at the giant-branch turnoff.
5. The timescale of energy injection varies from of order a single orbital period for a Jovian planet engulfed by a host near the turnoff, to 10^4 orbital periods at the tip of the giant branch. Minimum radius objects are short-lived with $N_{\text{decay}} \ll 1$.
6. Emergent luminosity will be mediated by transport through the optically thick stellar envelope and is not expected to match L_{decay} , particularly when $L_{\text{decay}} > L_*$.

While the engulfment of planets by their host stars is a common event in that many to most stars are subject to such an interaction during their lifetime, the present-day specific event rate is low, of the order of 0.1 – 1 yr^{-1} in the Galaxy. This fact motivates examination of the long-lasting observational signatures of companion interaction with a focus on stars ascending the lower giant branch with $L_* < 100 L_\odot$.

We gratefully acknowledge thoughtful and detailed feedback from the referee, C. Tout, and helpful discussions with A. Antoni, J. Grindlay, A. Loeb, C. Morley, K. Masuda, E. Ostriker, E. Ramirez-Ruiz, J. Stone, and S. Tremaine. Support for this work was provided by NASA through Einstein Postdoctoral Fellowship grant number PF6-170169

awarded by the *Chandra* X-ray Center, which is operated by the Smithsonian Astrophysical Observatory for NASA under contract NAS8-03060.

ORCID iDs

Morgan MacLeod  <https://orcid.org/0000-0002-1417-8024>
Matteo Cantiello  <https://orcid.org/0000-0002-8171-8596>
Melinda Soares-Furtado  <https://orcid.org/0000-0001-7493-7419>

References

- Aguilera-Gómez, C., Chanamé, J., Pinsonneault, M. H., & Carlberg, J. K. 2016a, *ApJL*, **833**, L24
Aguilera-Gómez, C., Chanamé, J., Pinsonneault, M. H., & Carlberg, J. K. 2016b, *ApJ*, **829**, 127
Alexander, J. B. 1967, *Obs*, **87**, 238
Carlberg, J. K., Cunha, K., Smith, V. V., & Majewski, S. R. 2012, *ApJ*, **757**, 109
Carlberg, J. K., Majewski, S. R., & Arras, P. 2009, *ApJ*, **700**, 832
Choi, J., Dotter, A., Conroy, C., et al. 2016, *ApJ*, **823**, 102
De Marco, O., & Soker, N. 2011, *PASP*, **123**, 402
Grether, D., & Lineweaver, C. H. 2006, *ApJ*, **640**, 1051
Howard, A. W., Marcy, G. W., Bryson, S. T., et al. 2012, *ApJS*, **201**, 15
Hoyle, F., & Lyttleton, R. A. 1939, *PCPS*, **35**, 405
Hut, P. 1980, *A&A*, **92**, 167
Joss, P. C., Rappaport, S., & Lewis, W. 1987, *ApJ*, **319**, 180
Kochanek, C. S., Adams, S. M., & Belczynski, K. 2014, *MNRAS*, **443**, 1319
Mayor, M., & Queloz, D. 1995, *Natur*, **378**, 355
Metzger, B. D., Giannios, D., & Spiegel, D. S. 2012, *MNRAS*, **425**, 2778
Metzger, B. D., Shen, K. J., & Stone, N. 2017, *MNRAS*, **468**, 4399
Meynet, G., Eggenberger, P., Privitera, G., et al. 2017, *A&A*, **602**, L7
Paczynski, B. 1976, in IAU Symp. 73, Structure and Evolution of Close Binary Systems, ed. P. Eggleton, S. Mitton, & J. Whelan (Dordrecht: D. Reidel), **75**
Paxton, B., Bildsten, L., Dotter, A., et al. 2011, *ApJS*, **192**, 3
Paxton, B., Cantiello, M., Arras, P., et al. 2013, *ApJS*, **208**, 4
Paxton, B., Marchant, P., Schwab, J., et al. 2015, *ApJS*, **220**, 15
Privitera, G., Meynet, G., Eggenberger, P., et al. 2016a, *A&A*, **591**, A45
Privitera, G., Meynet, G., Eggenberger, P., et al. 2016b, *A&A*, **593**, A128
Privitera, G., Meynet, G., Eggenberger, P., et al. 2016c, *A&A*, **593**, L15
Rasio, F. A., Tout, C. A., Lubow, S. H., & Livio, M. 1996, *ApJ*, **470**, 1187
Sandquist, E., Taam, R. E., Lin, D. N. C., & Burkert, A. 1998, *ApJL*, **506**, L65
Sandquist, E. L., Dokter, J. J., Lin, D. N. C., & Mardling, R. A. 2002, *ApJ*, **572**, 1012
Schlaufman, K. C., & Winn, J. N. 2013, *ApJ*, **772**, 143
Siess, L., & Livio, M. 1999a, *MNRAS*, **304**, 925
Siess, L., & Livio, M. 1999b, *MNRAS*, **308**, 1133
Soker, N., Livio, M., & Harpaz, A. 1984, *MNRAS*, **210**, 189
Soker, N. 1998, *AJ*, **116**, 1308
Soker, N., & Tytenda, R. 2006, *MNRAS*, **373**, 733
Staff, J. E., De Marco, O., Wood, P., Galaviz, P., & Passy, J.-C. 2016, *MNRAS*, **458**, 832
Valsecchi, F., & Rasio, F. A. 2014, *ApJ*, **786**, 102
van Dokkum, P. G., Leja, J., Nelson, E. J., et al. 2013, *ApJL*, **771**, L35
Villaver, E., & Livio, M. 2009, *ApJL*, **705**, L81
Winn, J. N., & Fabrycky, D. C. 2015, *ARA&A*, **53**, 409
Wright, J. T., Marcy, G. W., Howard, A. W., et al. 2012, *ApJ*, **753**, 160
Yamazaki, R., Hayasaki, K., & Loeb, A. 2017, *MNRAS*, **466**, 1421
Zahn, J.-P. 1977, *A&A*, **57**, 383
Zhang, M., & Penev, K. 2014, *ApJ*, **787**, 131